



Wind effects on the circulation of a geometrically-complex small estuary

Maria Jose Marin Jarrin^{a,b,*}, David A. Sutherland^a

^a Department of Earth Sciences, University of Oregon, Eugene, OR, USA

^b Facultad de Ingeniería Marítima y Ciencias del Mar, Escuela Superior Politécnica del Litoral, Guayaquil, Ecuador

ARTICLE INFO

Keywords:

Estuarine dynamics
Wind-driven circulation
Wind setup
Salinity
Velocity
Temporal variations

ABSTRACT

Local geometry and bathymetry set bounds on how estuarine circulation and salinity respond to river and tidal forcing. Although often considered secondary, wind can drive variations in the salinity field, as well as inducing locally strong along and across-estuary salinity and water level gradients. Here, we use observations and numerical simulations to look at the effect of winds on estuarine dynamics in the Coos Estuary in the Pacific Northwest. The small, strongly tidally-forced estuary, does not conform to the traditional funnel-shaped estuary, instead it is shaped like an inverted U. The numerical simulations use idealized forcing to separate the contribution of tides, river discharge, and winds, on subtidal salinity and velocity fields. We find that wind can lead to reversals in the out-estuary surface flow despite the tidal dominance on subtidal circulation, in accordance with the limited available observations. Northward winds pile fresher waters in the north side of the estuary, and decrease exchange flow due to the winds opposing the main channel surface outflow, which may ultimately enhance the transport of particles along estuary. Southward winds pile fresher waters on the southern sides of the estuary, where most of the flats are found, and act to enhance the loss of salt. These transient winds drive non-transient changes to salt content in the estuary: high discharge cases show a general increase of salt, while low and moderate discharge show a reduced loss of salt in the estuary after the winds are turned off. The wind-driven spatial and temporal variability quantified here in the salinity and velocity distribution underscores the importance of local geometry constraints on estuarine dynamics, especially as many estuaries continue to evolve either due to natural environmental changes or to anthropogenic impacts.

1. Introduction

Estuaries are the mixing zones between rivers and the coastal ocean, and are utilized for habitat and refuge by many organisms, such as oysters, crabs, fish, and phytoplankton (Cloern et al., 2017; Epifanio and Garvine, 2001; Garvine, 1991; Janzen and Wong, 2002; Sharples et al., 2017). Many species have adapted to the strong temporal and spatial gradients in salinity and temperature that exist within estuaries. The same drivers that set these hydrographic gradients can also directly affect a species' transport and survival within an estuary. For example, during 1997–1998, the Willapa Bay, WA, estuary received an increased amount of green crab larvae that was correlated to high river discharge (Yamada et al., 2005). Once introduced, this green crab population could then self-sustain due to relatively long retention in parts of the estuary (>1 month timescales) caused by a combination of tidal and channel curvature effects (Banas et al., 2009).

Subtidal (i.e., low-pass filtered to remove tidal variability) estuarine circulation is traditionally viewed as a balance between the along-

channel baroclinic pressure gradient and vertical mixing. The resulting steady flow is termed the gravitational circulation, or estuarine exchange flow, and sets the along-estuary gradients that dictate conditions felt by organisms on longer time-scales. Assuming a uniform horizontal density gradient and neglecting tidal variations, this exchange flow can be predicted for partially-mixed estuaries as a function of river discharge, tidal currents that act to mix the water column, and bathymetry (e.g., Hansen and Rattray, 1965; MacCready and Geyer, 2010). Many characteristics of real estuaries, however, complicate the simplified theory's assumptions. These include channel curvature (Chant, 2002; Geyer, 1993; Kranenburg et al., 2019; Lacy and Monismith, 2001) and strong temporal forcing (i.e., unsteadiness) due to tides, winds, discharge, or other factors. Indeed, in small (i.e., the length of salt intrusion is comparable to the tidal excursion), strongly tidally-forced estuaries, time dependence is an important factor, especially in estuaries where the discharge regime is on the same order as the estuarine response time (Banas et al., 2004; Bolaños et al., 2013; Conroy et al., 2020). Thus, understanding how variations in the estuarine circulation

* Corresponding author. Department of Earth Sciences, University of Oregon, Eugene, OR, USA.

E-mail address: mjmarin@espol.edu.ec (M.J. Marin Jarrin).

<https://doi.org/10.1016/j.ecss.2022.108092>

Received 24 September 2021; Received in revised form 15 September 2022; Accepted 27 September 2022

Available online 14 October 2022

0272-7714/© 2022 Elsevier Ltd. All rights reserved.

interact over a range of time scales is still needed, especially as applied to how estuarine flow influences biological patterns.

Wind forcing occurs over a large range of distinct time and space scales, including local diurnal winds (Uncles and Stephens, 2011), passing storms (Purkiani et al., 2016), seasonally-varying offshore winds (W. R. Geyer, 1997) that can drive upwelling/downwelling (Giddings and MacCready, 2017), and remote winds that create coastally-trapped waves that affect sea level (Hickey et al., 2016). During storm events, wind stress mixes the water column and reduces stratification (Blumberg and Goodrich, 1990; Li and Li, 2011); however, the same wind stress can modulate the estuarine exchange flow through vertical shear wind straining (Chen and Sanford, 2009; Scully et al., 2005). Additionally, the response of exchange flow to wind depends on the lateral bathymetry, where downwind flow on the shoals is produced by wind-driven flow, while in the channel upwind flow is produced (Chen and Sanford, 2009; Csanady, 1973; Lerczak and Geyer, 2004; Sanay and Valle-Levinson, 2005). This lateral variability can feed into the barotropic flow by changing sea level gradients locally (Nidzieko and Monismith, 2013). Hence, wind complicates the estuarine exchange flow conceptual model by adding unsteadiness, influencing stratification, and inducing horizontal gradients (Pfeiffer-Herbert et al., 2015; Xia et al., 2011; Xie and Eggleston, 1999). Although research examining the interaction of wind and estuarine circulation is not new, previous numerical studies have primarily used idealized geometries that ignore the realistic shape of many estuaries that alters their response to wind (e.g., Chen and Sanford, 2009; Coogan and Dzwonkowski, 2018; Purkiani et al., 2016). Here, we explore wind forcing on the observed circulation in the strongly-forced, geometrically-complex Coos Estuary, located in southern Oregon on the US West Coast, and expand our understanding across the entire estuary using a set of numerical model experiments.

2. Background

2.1. The Coos Estuary

Estuaries are found all over the coastal Pacific Northwest (PNW - Fig. 1) and the Coos Estuary is the second largest in terms of surface area and volume. The Coos Estuary is located south of Heceta Bank (Fig. 1a), inshore of a relatively narrow continental shelf (Hickey and Banas, 2003), and is home to ecologically important native species such as Olympia oysters (*Ostrea lurida*) and eelgrass (*Zostera marina*) (O'Higgins and Rumrill, 2007). The estuary shape is an inverted-U, due to a 4-km long bend centered around 15 km from the mouth. This torturous geometry is common among estuaries in the PNW. The main navigational channel is dredged annually from the mouth up to 24 km near the Coos River entrance to maintain 11 m of depth and 91 m of width (U.S. Army Corps of Engineers, 2015). Areas outside the channel consist primarily of tidal flats and subsidiary sloughs (Emmett et al., 2000; Groth and Rumrill, 2009). Tidal flats, with water depth ≤ 1.5 m, cover an area of approximately 15 km² or 30% of the estuarine area (Eidam et al., 2020).

Freshwater discharge into the estuary comes from numerous small creeks and rivers, with the largest flow from the South Fork Coos River that ranges from 2 m³ s⁻¹, in the dry season, to 800 m³ s⁻¹ (during storm events, Lee II and Brown, 2009; Sutherland and O'Neill, 2016). Discharge peaks are associated with storms that bring strong and shifting winds (Fig. 2). The lunar semidiurnal M₂ tidal height amplitude is about 0.8 m (averaged over a year), with mean tidal currents of 1.1 m s⁻¹ resulting in an average tidal excursion of 14 km (Baptista, 1989).

Previous observations show that the Coos Estuary salinity structure resembles a salt-wedge during high river discharge, a well-mixed estuary during low discharge, and a partially-mixed estuary during moderate discharge (Sutherland and O'Neill, 2016). Based on a year-long realistic numerical hindcast model, Conroy et al. (2020) found the Coos Estuary to be time-dependent, with local geometry driving important dispersive processes such as tidal trapping (lateral exchange at tributary

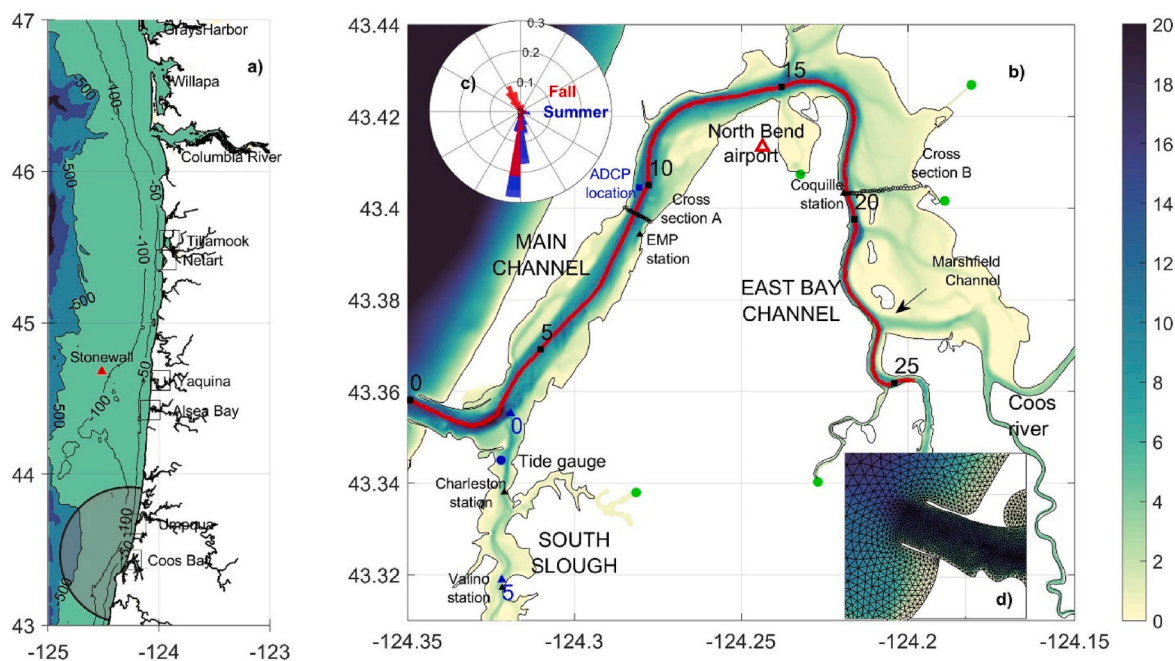


Fig. 1. a) Map of example PNW estuaries, indicating the Coos (model domain in black outline) and the location of the Stonewall buoy (red triangle). b) Zoom-in on the Coos Estuary, showing bathymetry (color) and the location of water quality monitoring stations (black triangles), meteorological station at the North Bend airport (red triangle), velocity stations (blue square), and tide gauge (blue circle). Black numbers and squares refer to distance (in km) from the mouth along the thalweg. Blue numbers and triangles show distance (in km) from the intersection of South Slough with the main estuary. c) Wind stress direction and magnitude ($N \cdot m^{-2}$) during the summer (blue) and fall (red) at the North Bend airport station. d) The unstructured FVCOM model grid at the mouth of the estuary where average horizontal resolution is 30 m. (For interpretation of the references to color in this figure legend, the reader is referred to the Web version of this article.)

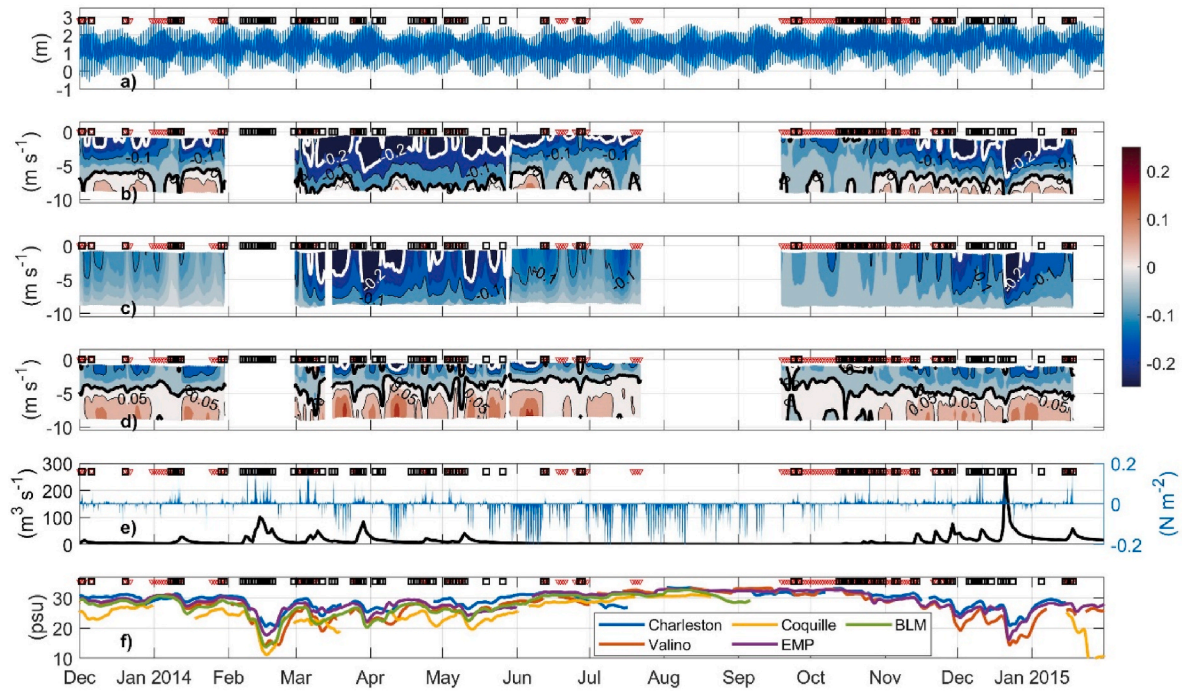


Fig. 2. a) Observed sea level (m) at the Charleston tide station (Fig. 1), (b) observed ADCP subtidal velocity at location shown in Fig. 1, blue colors show out-estuary and red colors show up-estuary (c) advective component of velocity calculated using Eq. 2, (d) density plus wind-driven components of velocity calculated by subtracting the barotropic component (c) from the ADCP measurements (b), using Eq. 2, (e) river discharge at South Fork (left axis) and meridional wind stress at the North Bend airport (right axis), (f) salinity at water quality stations located throughout the estuary. Red downward triangles at the top of each panel represent times when subtidal near-surface velocities (<1.3 m of depth) are weaker than -0.1 m s $^{-1}$, while black squares are shown at times when northward wind stress exceeds 0.1 N m $^{-2}$. (For interpretation of the references to color in this figure legend, the reader is referred to the Web version of this article.)

junctions) and jet-sink flow. Additionally, the model showed that the Coos Estuary has a tidally-driven exchange flow and salt flux that persists year-round, despite the seasonal changes in river discharge (Conroy et al., 2020). Large winter discharge events drive a mean flow that pushes salt out estuary, while in the dry summer, adjustment times are longer than summer itself, resulting in oceanic salinities up to 20 km landward. However, the model neglected wind.

Winds in the PNW blow primarily southward in the summer months of May through September (Fig. 1). These winds drive persistent summer upwelling along the coast, where surface waters move offshore and cold, salty, nutrient-rich waters move upwards and onshore towards the coast (Hickey and Banas, 2003). During the wet season (November to April) winds shift to northward on average, with the strongest winds associated with passing storms (Hickey and Banas, 2003). Additionally, during the summer a strong diurnal sea breeze blows eastward with wind stresses up to 0.3 N m $^{-2}$.

2.2. Theoretical background

To understand the way winds affect circulation in an estuary that is mostly tidally forced, we start with the momentum balance for a linear, quasi-steady, non-rotational and laterally invariant subtidal circulation (Geyer, 1997; Hansen and Rattray, 1965; Valle-Levinson et al., 2019), which is given by

$$A_z \frac{\partial^2 u}{\partial z^2} = g \frac{\partial \eta}{\partial x} + \frac{g}{\rho_0} \frac{\partial \rho}{\partial x} H, \quad (1)$$

where, A_z is the vertical eddy viscosity, u is the along-estuary velocity at depth z , g is the gravitational acceleration, η is the water elevation, ρ is the density and H is the water depth. Although the assumptions leading to Eqn. (1) are questionable for the Coos Estuary, due to its strong lateral gradients, we can still use it to qualitatively examine the separate influence of the horizontal density gradient and wind forcing. Eq (1) has a

solution of the form (Hansen and Rattray, 1965; Officer, 1976).

$$u(z) = \frac{3}{2} u_a \left[1 - \frac{z^2}{H^2} \right] - \frac{gH^3}{48\rho} \frac{\partial \rho / \partial x}{A_z} \left[9 \left(1 - \frac{z^2}{H^2} \right) - 8 \left(1 + \frac{z^3}{H^3} \right) \right] + \frac{H}{4\rho} \frac{\tau_{wx}}{A_z} \left[4 \left(1 + \frac{z}{H} \right) - 3 \left(1 + \frac{z^2}{H^2} \right) \right] \quad (2)$$

where τ is the wind stress, and u_a is the depth-averaged velocity. The first term describes the barotropic component that is driven by river discharge and sea level. The second term, the baroclinic pressure, describes the flow driven by density gradients, is sensitive to the water depth, and depends inversely on A_z (which depends on tidal forcing and stratification). The third term denotes the subtidal flow driven by wind stress and depends on depth and A_z . Using this solution, we can define the Wedderburn number (W) as the ratio of wind stress to baroclinic pressure gradient (Chen and Sanford, 2009; Geyer, 1997; Monismith, 1986):

$$W = \frac{\tau_{wx} L}{\Delta \rho g H^2}, \quad (3)$$

where L is the length of an estuary and $\Delta \rho$ is the horizontal density difference along the estuary.

3. Methods

3.1. Observations

Water velocity time series were collected from late 2013 until early 2015 using a bottom-mounted, upward-looking SonTek 150 kHz Acoustic Doppler Current Profiler (ADCP) provided by South Slough National Estuarine Research Reserve (SSNERR). The ADCP was located in the main channel seaward of the North Bend, close to the northern shoals, at about 10 m depth, hence these data potentially miss the

deepest landward flow in the channel (Fig. 1, Table 1). The top and bottom bins were excluded to eliminate surface and bottom effects. All velocity data were rotated to be oriented in the along-channel direction, corresponding to the principal component direction at each location.

Hourly tidal height time series were obtained from a NOAA tide gauge at Charleston, OR (Fig. 1). Subtidal variability was obtained using a low-pass Godin filter (consecutive 24–24–25 h filters), and sea level anomalies were calculated as deviations from the subtidal signal (high frequency signal). Tidal constituents from sea level were computed using the T-TIDE harmonic analysis software (Pawlowicz et al., 2002).

Water property data were obtained from 5 monitoring stations located throughout the estuary (Fig. 1b, Table 1). Salinity, temperature, dissolved oxygen and pH is measured every 15 min at all stations. We only discuss salinity here. The Charleston Bridge and Valino stations are telemetered to provide near real-time data access by SSNERR, at 3.0 and 5.6 km from the mouth inside South Slough, respectively (Fig. 1, Table 1). The Confederated Tribes of the Coos, Lower Umpqua and Siuslaw (CTCLUSI) monitor water quality at two additional stations: Bureau of Land Management (BLM) and Empire Docks (EMP), with data available from 2011 to present at distances of 8.1 and 6.9 km from the mouth, respectively (Fig. 1, Table 1). Beyond North Bend, the Coquille Indian Tribe monitor a station 18 km from the mouth (Coquille WQ). Finally, along-estuary hydrography in the estuary was described by Sutherland and O'Neill (2016), from conductivity-temperature-depth (CTD) profiles collected during 2012–2014.

River discharge data from the South Fork Coos River gauge (Fig. 1, Table 1) from 2003 to present was used as a proxy for the total freshwater input to the estuary (Baptista, 1989). Although there are more than 13 sources of freshwater input, the Coos River is the main source of freshwater to this system (~66% of total discharge), of which the South Fork is the main component (Conroy et al., 2020).

Wind velocity data were extracted from a meteorological station at the North Bend Southwest Oregon Regional Airport (Fig. 1, Table 1). We use oceanographic wind convention. Importantly, northward winds correspond to up-estuary winds in Main Channel before the bend (Fig. 1), yet, they are down-estuary in the East Bay Channel (beyond the bend). For comparison with the shelf, winds at the Stonewall Buoy (Fig. 1, Table 1) are also obtained for the time span of the study.

Table 1

Oceanographic and meteorological stations analyzed in this study with locations shown in Fig. 1. Instrument height above bottom (HAB) is shown, along with mean water depth (m) and distance from the estuary mouth (km).

Station	Institution	Time range	Depth (m)/ HAB (m)	Distance (km)
Water quality stations				
Valino Island	SSNERR	1999–	2.4/0.5	5.6
Charleston	SSNERR	2002–	4.0/0.5	3.0
EMP	CTCLUSI	2011–2014	6.0/0.5	6.9
BLM	CTCLUSI	2011–2014	5.0/0.5	8.1
Coquille	Coquille Tribe	2013–2017	11.9/0.5	18
Water velocity data				
ADCP location	SSNERR	2013–2015	10.5/9.5	10.0
Sea level from tide gauge				
Charleston 9432780	NOAA	1991–	3.0/–	3.0
River discharge				
South Fork at Coos river 14323600	CoosWa	2003–	44 (elev.)	49
Meteorological stations (wind magnitude and direction)				
North Bend airport	NOAA	1949–	5.1 (elev.)	12.5
	24284			
Stonewall buoy	NOAA	1991–	3.8 (elev.)	147.5
	46050			

3.2. Numerical simulations

3.2.1. Model setup and validation

We use the Finite Volume Coastal Ocean Model (FVCOM) to simulate the impact of winds on the circulation in the Coos Estuary. FVCOM is a prognostic, finite-volume, free-surface, three-dimensional primitive equation model with an unstructured grid (Chen et al., 2003, 2018; Huang et al., 2008; Qi et al., 2009). FVCOM was chosen because it resolves tidal elevations, water properties, and currents in areas with complex topographical features and has a robust wetting/drying scheme. The model domain covers the entire estuary with an open boundary well outside the mouth of the estuary (Fig. 1a). The horizontal grid has a spatial resolution that varies from ~30 m within the bay to ~3 km at the outer boundary (other model parameters are specified in Sup. Table 1) The vertical coordinate has 20 levels in a uniform hybrid terrain-following grid. The model bathymetry within the estuary was interpolated from 2014 USGC Coastal LiDAR data and in-situ single-beam echosounder surveys (Conroy et al., 2020). Model boundary conditions include idealized tidal forcing at 52 open boundary nodes (Fig. 1), using only the M_2 semidiurnal tidal constituent extracted from the Charleston tide gauge. Using only one tidal constituent allows us to understand the impact of the subtidal variability (spring/neap water level) on baroclinicity needed to be overcome by wind forcing. The simulations were initiated with a 1-month spin-up period for each forcing scenario, which were then subsequently used as initial conditions for each wind-event case. For all runs, the initial salinity equaled 34, while a salinity of 0 was imposed at the river input locations. This set up is similar to previously validated realistic hindcast simulations Conroy et al. (2020); Eidam et al. (2020). However, to save computational time, we use a slightly coarser horizontal resolution (up to a factor of 2 inside the estuary), and conduct a qualitative validation (see results) to ensure the model reproduces the main estuarine characteristics.

3.2.2. Model experiments

To investigate the dependence of estuarine circulation on wind strength and direction, we designed a set of six baseline simulations in which tidal forcing and river discharge (Q_r) are held steady for 30 days at representative magnitudes: Base Cases. Two fixed tidal amplitudes represent the fortnightly variability: an amplitude of 0.79 m for neap tides and 1.17 m for spring tides. We vary Q_r to mimic the seasonality: 1) High (rain event during the wet season), 2) Moderate (mean wet season), and 3) Low (mean dry season). The high discharge case uses a South Fork Coos River discharge of $187 \text{ m}^3 \text{ s}^{-1}$, which is exceeded ~25% of the time during a typical year. We use $19 \text{ m}^3 \text{ s}^{-1}$ for the moderate case, which occurs 45% of the time in an average year, and $Q_r = 1.5 \text{ m}^3 \text{ s}^{-1}$ for the low discharge case, representing the remaining roughly 30% of time in a given year.

Using Eq. (3), we calculate the wind stress needed to balance the baroclinic pressure gradient force, with a mean water depth $H = 10 \text{ m}$. Based on hydrographic sections (Sutherland and O'Neill (2016), the estuary length $L = 14 \text{ km}$, while the salinity gradient varies from $5 \text{ psu}\cdot\text{km}^{-1}$ (rainy season) to $1 \text{ psu}\cdot\text{km}^{-1}$ (dry season). Using this relationship, we estimate that a τ_{wx} of $0.2 \text{ N}\cdot\text{m}^{-2}$, a typical storm-related magnitude, is comparable to the baroclinic pressure gradient. We develop experiments using two wind stress magnitudes, $0.2 \text{ N}\cdot\text{m}^{-2}$ and $0.1 \text{ N}\cdot\text{m}^{-2}$, and two spatially-uniform wind directions, northward and southward. Hence, we have 24 total wind simulations to test the effect of four distinct wind types (weak and strong northward winds, and weak and strong southward winds) across the typical seasonal span of tidal and river forcing represented by the Base Cases (Sup. Table 2).

3.3. Data analysis

We employ an along/across estuary coordinate system for both observations and model output based on the local orientation of the channel thalweg. In this coordinate system, the along-estuary

component is positive landwards. In the first 15 km, the estuary is parallel to the coast (in what we will call Main Channel, km 4 to 15) at which point it reverses direction around a U-shaped bend (North Bend). We define two cross-sectional transects (Fig. 1) to explore the circulation before the bend (Cross section A), and after the bend (Cross section B). The channel portion landward of the bend will be referred to as East Bay Channel (km 15 to 22).

To explore the subtidal variability, we apply a 24-24-25 h Godin filter to all the time series used. Hourly model outputs were further processed by averaging 2 days before the wind events, to obtain the “pre-event” values, and the 2 days during the wind forcing for the “event” analysis. Anomalies are calculated as event minus pre-event values. We define the salinity gradient as the difference between the salinity at the mouth (S_{mouth}) and any distance along the thalweg at distinct depths. Stratification (ΔS) is calculated by differencing the surface and bottom values of modeled salinity fields, which along with along-estuary gradients can be affected by the lateral structure of salinity (Geyer et al., 2020).

4. Results

4.1. Observed estuarine conditions

We examine observed estuarine water properties, circulation, and forcing over two winter seasons and one summer season (Fig. 2). The subtidal along-estuary velocity exhibits a clear two-layer pattern (Fig. 2b), with down-estuary velocities at the surface and up-estuary velocities deeper than 7 m (Fig. 3a). The upper several meters have velocities of $-0.19 \text{ m}\cdot\text{s}^{-1}$, with faster speeds ($-0.21 \text{ m}\cdot\text{s}^{-1}$) related to rain events in spring, summer and winter, at a cross-correlation lag of 31 h from the peak discharge (Figs. 2e and 3a). The calculated barotropic component using Eq. (2) (Figs. 2c and 3a), shows a unidirectional out-estuary flow, with stronger negative velocities at the surface during high discharge ($R^2 = 0.5$).

We calculated the density-driven plus wind-driven flow by

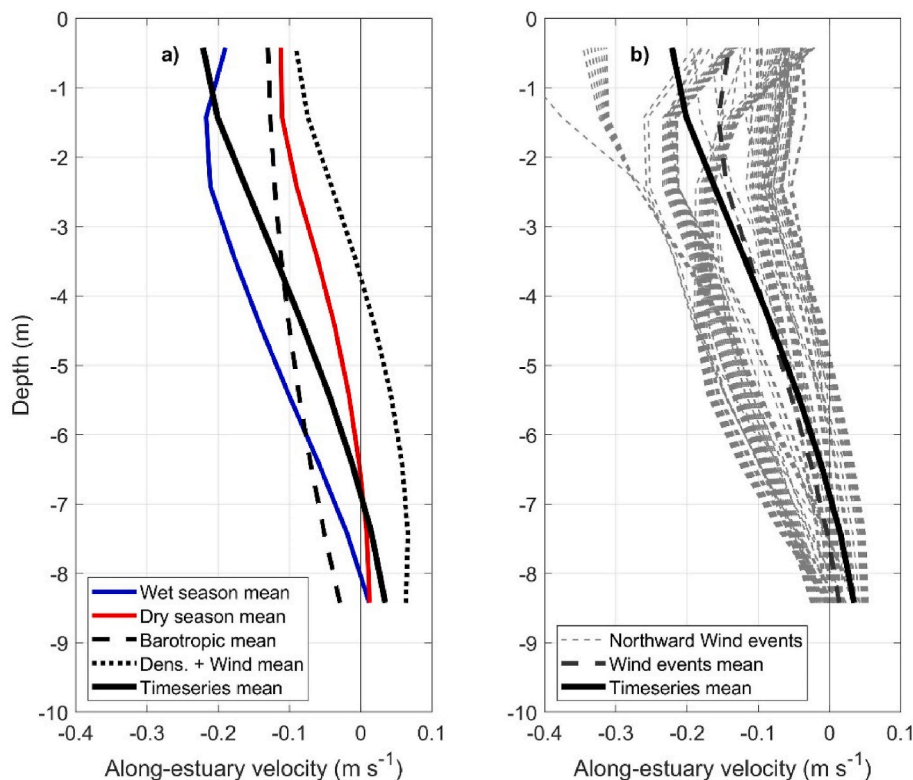


Fig. 3. a) Subtidal velocity profiles from the ADCP location during high discharge (blue), during the dry season (red), and time series mean (black). Time series’ barotropic component mean (broken line) and density + wind-driven component mean (dotted line) are also shown. b) Velocity profiles during northward wind events (thin gray lines), the wind-events mean profile (thick gray), and the overall time series mean (black). (For interpretation of the references to color in this figure legend, the reader is referred to the Web version of this article.)

subtracting the barotropic component from the ADCP measurements (Eq. (2); Fig. 2d). Though the magnitude of the velocity of this residual depends on the choices of eddy viscosity (A_z) in the baroclinic and density-driven components (Eq. (2)), the vertical distribution depends on the magnitude of horizontal pressure gradient and wind stress (Geyer, 1997). This residual field highlights the bidirectional flow, with out-estuary velocities at the surface averaging $-0.07 \text{ m}\cdot\text{s}^{-1}$ ($\pm 0.04 \text{ m}\cdot\text{s}^{-1}$ standard deviation), and up-estuary flow at depth of $0.06 \text{ m}\cdot\text{s}^{-1}$ ($\pm 0.04 \text{ m}\cdot\text{s}^{-1}$ standard deviation). During discharge events (Fig. 3a), the whole water column moves in the out-estuary direction at the ADCP location. During the dry season (Fig. 3a), surface layer along-estuary velocities decrease to their minimum values ($-0.10 \text{ m}\cdot\text{s}^{-1}$, Fig. 3a). A clear spring-neap modulation is also present in the subtidal flow (Fig. 2c).

Salinity varies seasonally in the estuary (Fig. 2f), with relatively large magnitude freshening events detected in Main Channel (Coquille, BLM, Charleston) that coincide with discharge events between November and May (Fig. 2e). The highest salinity values (>30) occur from July to October as the estuary accumulates salt due to reduced freshwater input. Higher salinities are also related to coastal upwelling events, e.g., in June 2014. CTD profiles show the water column to be strongly stratified in salinity close to the ADCP location during the rainy months (Sutherland and O’Neill, 2016), while during the drier months, stratification is reduced. Based on the CTD surveys, the observed along-estuary salinity gradient is positive in the rainy months (i.e., salt decreasing up estuary), while during the dry months these gradients are reduced and sometimes reversed, related to freshwater input from side channels (a, Conroy et al., 2020).

4.2. Observed wind events and estuary response

We find that the seasonally changing N-S wind component at the offshore Stonewall buoy (about 120 km away from the mouth of the estuary) is significantly correlated to the sea level anomaly at the Charleston tide gauge ($R^2 = 0.45$, at 18 h of lag, with wind leading sea

level), with positive anomalies during storms, and negative anomalies in the upwelling season during southward wind peaks (Sup. Fig. 1). Local winds follow these large-scale trends (Sup. Fig. 1), except in areas blocked by topography such as the North Bend airport, where northwards winds are not registered during the winter, yet a strong correlation is found between the two meteorological stations ($R^2 = 0.62$ with a 7-h lead).

Using the ADCP time series we find a total of 129 days when the subtidal out-estuary upper layer flow in Main Channel was reduced to at least $-0.15 \text{ m}\cdot\text{s}^{-1}$ (red triangles in Fig. 2). About 1/3 of these events (44 out of 129) were preceded by a change in wind direction from southward to northward (highlighted with black squares in Fig. 2). Correspondingly, subtidal salinities (Fig. 2f) show a slight increase with the change in wind direction, followed by a strong decrease as Q_r increases, since the storms also bring heavy precipitation. Velocity profiles during northward wind events (Fig. 3b) show a reduction in out-estuary speed in the upper 5 m of the water column. This depth-varying effect suggests the importance of the opposing wind stress, possibly modified by additional barotropic effects (sea level set-up). The duration of the northward wind events is approximately 1–2 days.

We use an example northward wind event to show the effects of τ_{wx} on the circulation of the Coos Estuary (Fig. 4a, e, i). From 3 to 5-May-2014, τ_{wx} is mainly northwards and peaks near $0.15 \text{ N}\cdot\text{m}^{-2}$, while tides transition from spring to neap (Fig. 4e). Q_r is relatively constant at $10 \text{ m}^3\cdot\text{s}^{-1}$, until 8-May when it increases to about $40 \text{ m}^3\cdot\text{s}^{-1}$ at the same time a second wind event is observed. Surface subtidal velocity in Main Channel over this time period (Fig. 4a) varies between -0.3 and $-0.1 \text{ m}\cdot\text{s}^{-1}$, with the weakest out-estuary velocities during the wind event. Subtidal salinity fluctuations also respond to the decrease in out-estuary velocities with a salinity increase of 0.3 in Charleston, 0.15 in EMP and 0.5 in Coquille (Fig. 4i). During the second wind event, a 0.1 salinity increase is registered in Charleston, 0.6 in EMP, and 1.9 in Coquille, until the discharge increases.

The wind record shows 51 events in which wind direction is southward during at least one day (Fig. 2e). Southward winds within the estuary act in the same direction as exchange flow in Main Channel and opposite to the exchange flow in East Bay Channel. Velocity profiles at the ADCP location during southward wind events (Fig. 2c) show a stronger out-estuary speed in the upper 5 m and stronger up-estuary speed at depth.

For the southward wind cases, we show an example from 18-May to 27-May (Fig. 4). In this case, Q_r does not drastically change during the selected period, while τ_{wx} transitions to upwelling-favorable (southward) starting on 20-May, albeit with a strong diurnal variability (Fig. 4g). Velocities in this period show an increase at depth in the up-estuary direction with a peak of $0.05 \text{ m}\cdot\text{s}^{-1}$ on 21-May (Fig. 4c). At the surface, out-estuary velocities strengthen from -0.2 to $-0.4 \text{ m}\cdot\text{s}^{-1}$. Salinity in the estuary initially decrease when winds change direction, but then increases steadily during the upwelling-favorable conditions (Fig. 4k).

The magnitude of the wind's effect on estuarine circulation is modulated by tidal cycle as reductions in surface velocity occur more frequently during neap tides and transitions (87% of all events, Fig. 2). However, despite this qualitative indication that reversal events occur more often during neap tides, it is difficult to disentangle the separate effects of wind, tidal influence, and river discharge on the observed subtidal flow from one location. Thus, we turn to the numerical simulations to examine the spatio-temporal influence of wind stress on the entire estuary.

4.3. Numerical simulations

4.3.1. Simulated estuarine conditions: qualitative validation

We find a general agreement between observed and no-wind simulated estuarine dynamics, as evidenced by the behavior of the salt intrusion as a function of river flow (Fig. 5b). Salinity gradients are

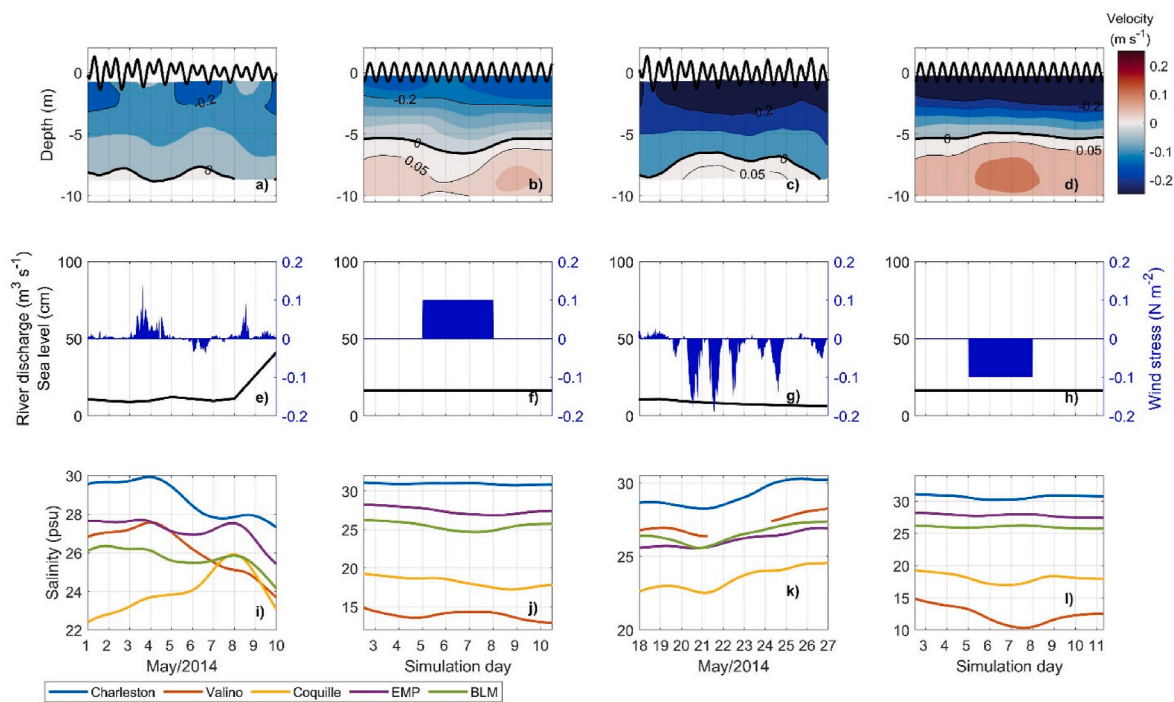


Fig. 4. Comparison of observed and modeled conditions in the Coos Estuary during northward (1–10-May-2014) and southward (18–27-May-2014) wind events. (a) Observed subtidal along-estuary water velocity ($\text{m}\cdot\text{s}^{-1}$) at the ADCP location, from observations. (b) Same as in a, but from model output. (c) Same as in a, but observed during southward winds. (d) Same as in c, but from model output. (e) Observed South Fork discharge (black) and wind stress. (f) Same as in e, but from model input. (g) Same as in a, but observed during southward winds. (h) Same as in g, but from model input. (i) Observed salinity at three sites in Main Channel and South Slough. (j) Same as in i, but from model output. (k) Same as in i, but observed during southward winds. (l) Same as in k, but from model output. Notice the y-axis is different for all salinity plots. See Fig. 1 for location of stations.

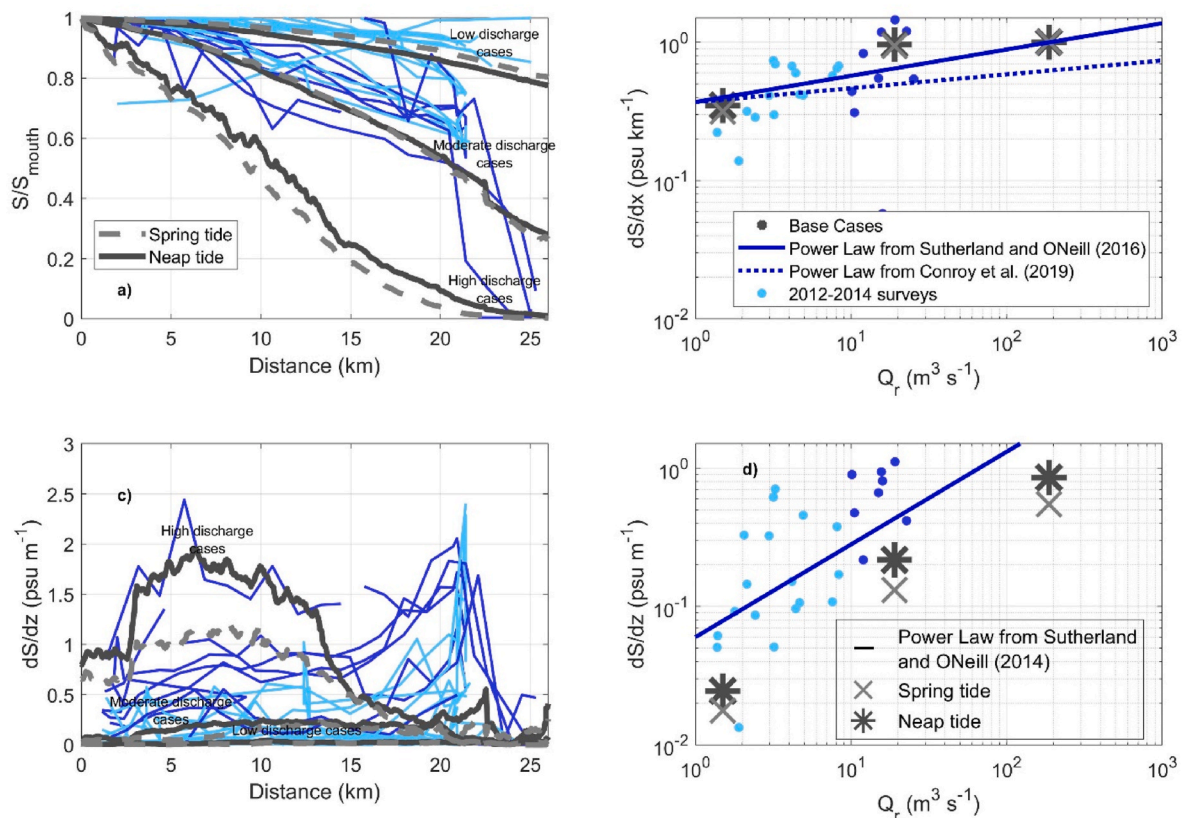


Fig. 5. Base Case (no-wind) experiments vs. 2012–2014 surveys. a) Depth-averaged salinity (S) normalized by the observed salinity at the mouth (S_{mouth}) as a function of along-estuary distance for the Base Cases (gray lines) and survey transects (colored by discharge – see Fig. 5b). b) Along-estuary salinity gradient for each Base Case (in gray crosses and asterisks) and observations (colored by discharge – see Fig. 5b) as a function of river discharge, Q_r . Black line shows a power law fit based on previous studies. c) Vertical stratification as a function of along-estuary distance for Base Cases (in gray crosses and asterisks) and surveys (colored by discharge – see Fig. 5b). d) Vertical stratification for Base Cases (in gray crosses and asterisks) and surveys (colored by discharge – see Fig. 5b), as a function of Q_r . Black line shows a power law fit based on previous studies.

relatively small across the low discharge cases, similar to the observed salt structure (Fig. 5b). Observed and modeled stratification fall in a similar magnitude range, with increases in stratification related to increases in river discharge (Fig. 5c). Under high discharge ($187 \text{ m}^3 \text{ s}^{-1}$, at the Coos River, Sup. Table 2), stratification in Main Channel reaches maximum levels ($1.5 \text{ psu} \cdot \text{m}^{-1}$), where salty water enters the estuary due to the density gradient. Both the stratification and salinity gradient as a function of river discharge agree with the observed power law variability found previously by Sutherland and O'Neill (2016) (Fig. 5d).

The model matches observations of velocity and salinity at the ADCP location (Fig. 4), and agrees with the previously validated, realistic simulations (Conroy et al., 2020). The subtidal along-channel velocity has a two-layer structure throughout the simulated time periods (Fig. 4b, d), showing stronger magnitudes during spring tides and high discharge forcing, similar to the high-resolution model (not shown). Though the model shows slightly higher velocity magnitude at depth, the general structure of a two-layer flow is observed throughout the time-series (Fig. 4b, d). Similar to Conroy et al. (2020), the coarser resolution model also has a mean fresh bias during the dry season, though this does not significantly affect the along-estuary salinity gradient. Due to this fresh bias, the simulated salinity magnitudes do not match the observations (Fig. 4), most likely due to the idealized nature of the model forcing. Despite these small differences, the model results give us confidence in using it to understand wind effects on the estuarine salinity fields and circulation.

4.3.2. No wind (Base) Cases

We use the no-wind Base Cases to characterize the circulation,

salinity field, and stratification across the estuary over a range of tidal and discharge forcing. We find the strongest out-estuary velocities along the thalweg during high discharge conditions with an up-estuary flow only below 8 m depth (Fig. 6a). During moderate and low discharge cases, velocities are in general smaller, with a shallower location at which velocities change direction (5 m, Fig. 6d and g, Sup. Fig. 2). This response is similar to that observed at the ADCP location (Fig. 3). In response to this velocity pattern, salinity varies significantly with river forcing, affecting both stratification and along-estuary gradient (Fig. 6). During high discharge, stratification is increased along the estuary (Fig. 6a), with nearly fresh water reaching Marshfield Channel ($S < 3$, 23 km from the mouth). Higher stratification is observed in Main Channel ($1.59 \text{ psu} \cdot \text{m}^{-1}$ during neap, $0.98 \text{ psu} \cdot \text{m}^{-1}$ during spring tide) while in East Bay Channel, stratification is reduced ($0.31 \text{ psu} \cdot \text{m}^{-1}$ during neap, $0.24 \text{ psu} \cdot \text{m}^{-1}$ during spring tide). During moderate and low discharge, stratification decreases (0.22 and $0.25 \text{ psu} \cdot \text{m}^{-1}$ on average over the estuary, respectively, Fig. 6).

At the surface, subtidal flow under moderate discharge is directed along the thalweg, with stronger velocities under the neap tide conditions (Fig. 7a) than during spring tides for the moderate discharge case (Sup. Fig. 3). The out-estuary flow curves around both North Bend and estuary mouth, converging towards the deeper parts of the channel. During the moderate and low discharge cases, out-estuary velocity is weaker than the high discharge experiments, allowing for salinities of 30 to be registered at the surface further up the estuary (4 km in the moderate discharge case and 16 km in the low discharge case - Fig. 6), and decreasing stratification.

The cross sections indicate that circulation in the estuary is more

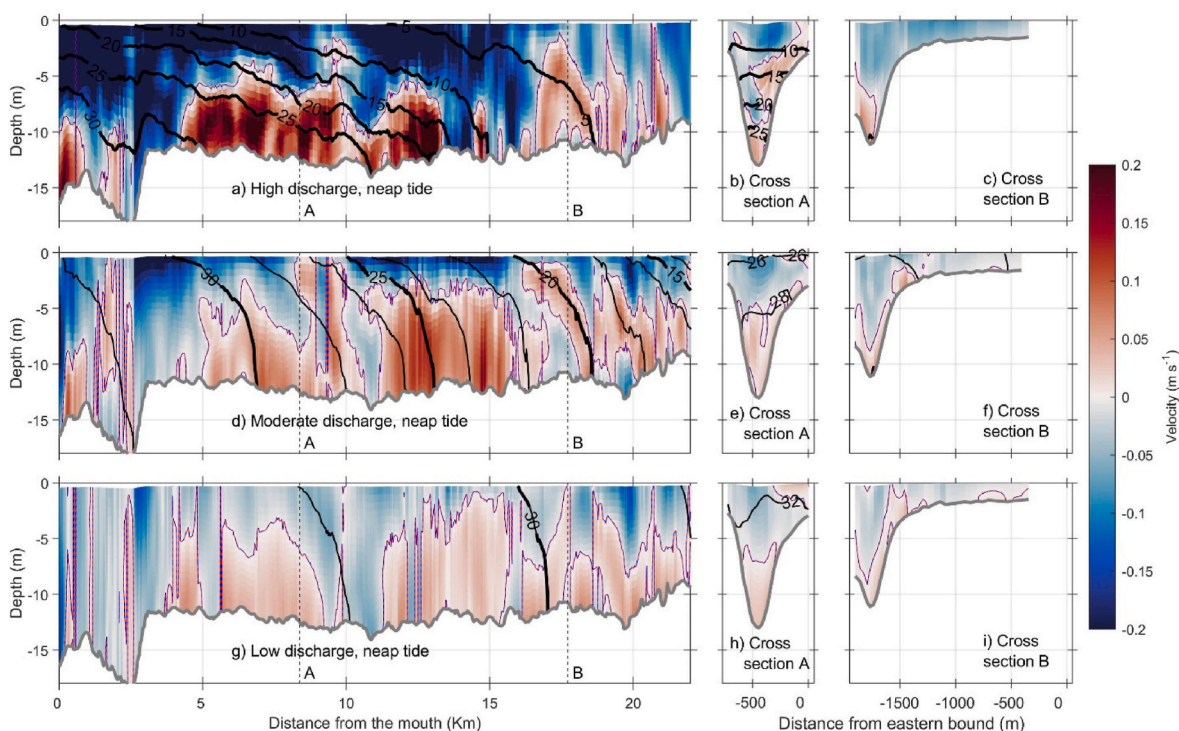


Fig. 6. Salinity and along-estuary velocity distribution along the thalweg for the no-wind Base Cases under neap amplitude forcing and the three river discharges. (a) Subtidal along-estuary water velocity (color) and salinity (contours) along the thalweg, under high discharge. (b, c) Subtidal along-estuary water velocity (color) and salinity (contours) at Cross sections A and B, under high discharge. (d) Same as a, but for moderate discharge. (e, f) Subtidal along-estuary water velocity (color) and salinity (contours) at Cross sections A and B, under moderate discharge. (g) Same as a, but for low discharge. (h, i) Subtidal along-estuary water velocity (color) and salinity (contours) at Cross sections A and B, under low discharge. Location of Cross sections are shown in Fig. 1. (For interpretation of the references to color in this figure legend, the reader is referred to the Web version of this article.)

complex than the typical 2-layer flow. For example, under high discharge, flow in Main Channel is laterally sheared (Fig. 6b), while under lower discharge flow has a stronger vertical variability (Fig. 6e, h). This produces salinity slightly enhanced on the eastern side, while the flow on the thalweg has lower salinities (Fig. 7a). These differences are observed in East Bay Channel as well, where up-estuary velocity is observed in the thalweg and out estuary velocity is observed over the flats (Fig. 6c, f, i). Lateral salinity gradients, induced by differential advection, can affect the along-estuary gradient and stratification, and in turn the effect that winds can have on estuarine circulation.

4.3.3. Simulated wind events and estuarine response

a) Northward wind events

Wind stress towards the north produces increased surface flow in the same direction, which in Main Channel is up-estuary, against the expected estuarine surface outflow, and in East Bay Channel and South Slough is out-estuary (Fig. 7b). This anomalous flow pattern leads to accumulation of fresher waters in North Bend. Our observations at the ADCP location, just south of the bend, agree with the results of our idealized experiments: an average decrease in salinity and velocity is observed at a time related to the change from no-wind to increased wind (Fig. 4).

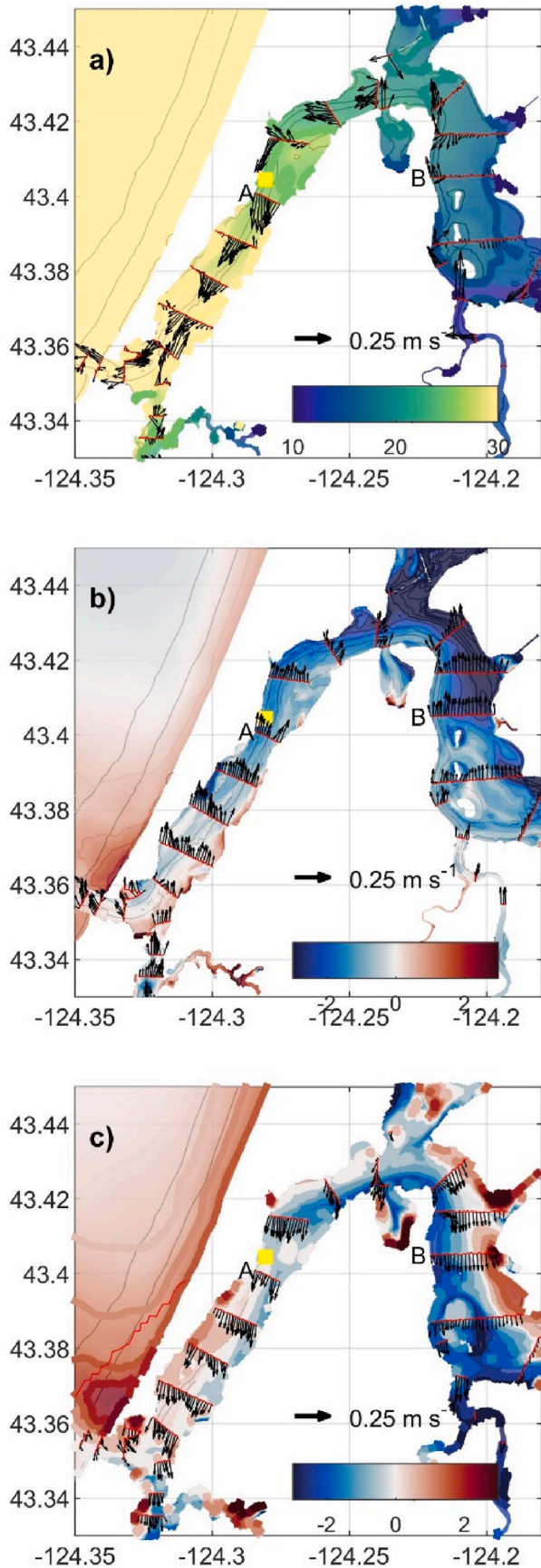
The full extent of our model allows us to explore the spatially-variable response to wind forcing of salinity and velocity, mainly due to the inverted U-shape of the Coos Estuary. We illustrate the overall estuarine response by focusing on the moderate discharge case with neap tides, as many of the features are shared across all forcing ranges, and discuss the other cases where important differences emerge.

In the first few kilometers of Main Channel, salinity at the surface increases along the southern edge up to 7.5 km from the mouth (Fig. 7b)

due to wind straining (1–6 m of depth). In this area, fresher water is observed along the northern side, where out-estuary velocities are reduced (anomalies shown in black arrows in Fig. 7b). In response to reduced velocities at the surface, exchange flow at depth is reduced as well (0.05 m s^{-1} slower), producing fresher deep waters at the entrance of the estuary. In East Bay Channel, wind is in the same direction as exchange flow at the surface, and small positive anomalies are observed in the surface velocity field (northward arrows in Fig. 7b). The freshest waters at the surface (4.5 fresher than Base Case) are accumulated on the northern side of North Bend, due to the enhanced surface flow from both sides of the bend pushing the less-dense waters in this direction. This produces an increase of water level of 0.8 cm under high discharge (average anomaly in North Bend), while under moderate and low discharge, water level increases 0.2 cm and 0.1 cm, respectively. The general distribution of surface salinity anomalies is similar between spring (not shown) and neap tides; however, salinity anomalies are greater during neap tides due to enhanced stratification (Fig. 8a).

Cross sections in the estuary show that the impact of winds on the Coos Estuary is not symmetrical: at Cross section A (Fig. 9b), slower out-estuary velocities are observed in the upper layer, while at depth up-estuary velocities are strengthened. Salinity is reduced at all levels, with greatest negative anomalies at the surface (-1.5). On the East Bay Channel Cross section (B - Fig. 9c), out-estuary flow above the thalweg is enhanced at the surface due to winds forcing in the same direction as exchange flow. On the flats, the out-estuary flow is slightly reduced producing the fresher water mass observed in Fig. 7b.

Cumulatively, the impact of winds on salinity and velocity in the Coos Estuary is fundamentally influenced by the estuarine geometry and bathymetry (Fig. 8). Strong northward winds increase the along-estuary depth-averaged salinity gradient under all river discharge cases and neap tide conditions. In the high river discharge case, the salinity gradient decreases 0.25 and 0.14 psu km^{-1} in Main Channel and East



(caption on next column)

Fig. 7. (a) Subtidal surface velocity (arrows) and surface salinity (contours) during neap tides and moderate discharge, averaged over 2 days for no winds (Base Case). (b) Subtidal surface salinity anomalies (event minus pre-event values in contours) and surface velocity anomalies (arrows) during weak northward wind event. (c) Same as b, but for the weak southward wind event. Location of the ADCP is marked with a yellow square. (For interpretation of the references to color in this figure legend, the reader is referred to the Web version of this article.)

Bay Channel, respectively. This difference in $\partial S/\partial x$ under high discharge is mostly driven by changes in the surface salinity (Fig. 7b). In the moderate discharge case, salinity gradient increases $0.18 \text{ psu}\cdot\text{km}^{-1}$ in Main Channel, while in East Bay Channel it increases $0.07 \text{ psu}\cdot\text{km}^{-1}$ (Fig. 8b). Finally, in the low discharge cases, a difference of $0.05 \text{ psu}\cdot\text{km}^{-1}$ and $0.0009 \text{ psu}\cdot\text{km}^{-1}$ is observed in Main Channel and East Bay Channel, respectively.

Stratification can be affected by winds via two methods: mixing and straining. Due to wind straining, northward winds accumulate fresher waters in North Bend, while at depth saltier waters are found close to the mouth and fresher waters in East Bay Channel (Fig. 9a). This produces a slight increase in stratification in Main Channel of $0.003 \text{ psu}\cdot\text{m}^{-1}$ (Fig. 8c–d), while in East Bay Channel stratification decreases by $0.04 \text{ psu}\cdot\text{m}^{-1}$, under moderate discharge. The strong stratification observed in the high discharge Base Case in Main Channel increases under wind forcing ($0.03 \text{ psu}\cdot\text{m}^{-1}$), while in East Bay Channel winds produce a decrease of stratification of $0.13 \text{ psu}\cdot\text{m}^{-1}$ (Fig. 8a–b). The low discharge Base Cases have the highest salinities throughout the water column. When northward winds are applied to that same low discharge case, stratification increases a small amount ($0.01 \text{ psu}\cdot\text{m}^{-1}$) in Main Channel and a negligible amount in East Bay Channel (Fig. 8e–f).

Temporal changes to salinity averaged over the whole estuary volume are shown in Fig. 10. Before winds are applied, the estuary is losing salt under high and moderate discharge. As northward winds are applied, fresher water is accumulated around North Bend, which slightly increases salinity due to a reduced advective salt loss as winds are in opposite direction. This slight increase of salinity continues after the winds are turned off due to the remaining increase in salt at depth (Fig. 9a). Increased salinity beyond North Bend (Fig. 8d) allows the estuary to increase salinity after the winds are turned off in the low discharge cases (Fig. 10c).

b) Southward wind events

Our numerical model results show that southward winds produce an enhanced outflow of fresher water at the surface, creating significant lateral and temporal variability, similar to the observations. At the ADCP location (Main Channel), winds act in the same direction as surface flow, strengthening exchange flow at the surface, while at depth, velocities become more landward due to upwelling at the coast, again similar to observations (Fig. 4).

Southward winds move fresher waters away from North Bend and towards the southeastern side of Main Channel and western side of East Bay, where the thalweg is located (Fig. 7c). The lateral gradient in velocity due to flow following the thalweg produces reduced salinity on the western side of Main Channel, observed at Cross Section A (Fig. 9b). Increased out-estuary flow at the surface in Main Channel is accompanied by enhanced up-estuary velocity at depth, which produces higher salinities at depth in Main Channel. In East Bay thalweg, fresher waters are observed (1.5 fresher) due to reduced exchange flow which decreases the inflow of salty waters in the thalweg, while on the shallow flats the output of freshwater is moved towards Marshfield channel, producing slightly higher salinities (1.38, Fig. 9f). This transport of waters south from both sides of the Bend produce in the moderate discharge case, a set down of 1.4 cm in the area (1.2 cm under high discharge and 1.5 cm under low discharge forcing).

As the length of the estuary changes with river discharge (Fig. 5), the

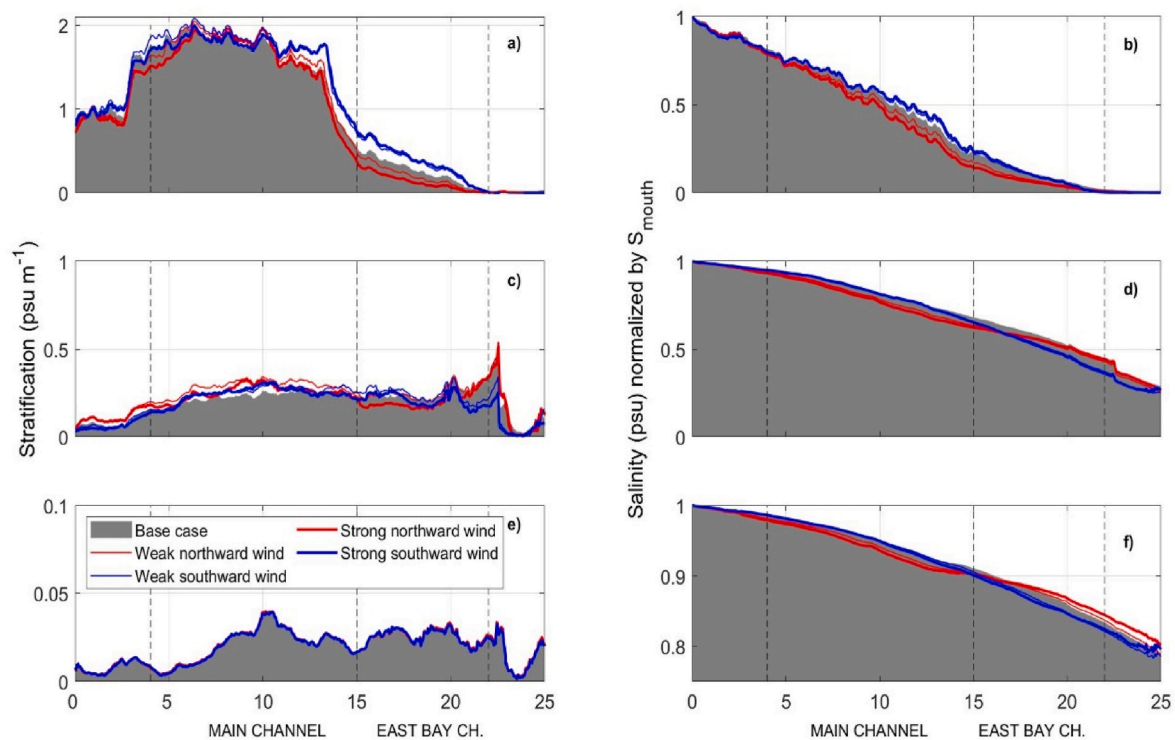


Fig. 8. Stratification (surface minus bottom salinity) along the thalweg under neap tide for Base Cases (gray), northward winds (red) and southward winds (blue) for a) high, c) moderate and e) low discharge. Depth-averaged salinity (normalized by salinity at the mouth) under neap tide for Base Cases (gray), northward winds (red) and southward winds (blue) for b) high, d) moderate and f) low discharge. Width of lines dependent on strength of wind forcing. Note the range of stratification and salinity gradient is constrained to see variability landward of the mouth. Broken lines show Main Channel and East Bay Channel area. (For interpretation of the references to color in this figure legend, the reader is referred to the Web version of this article.)

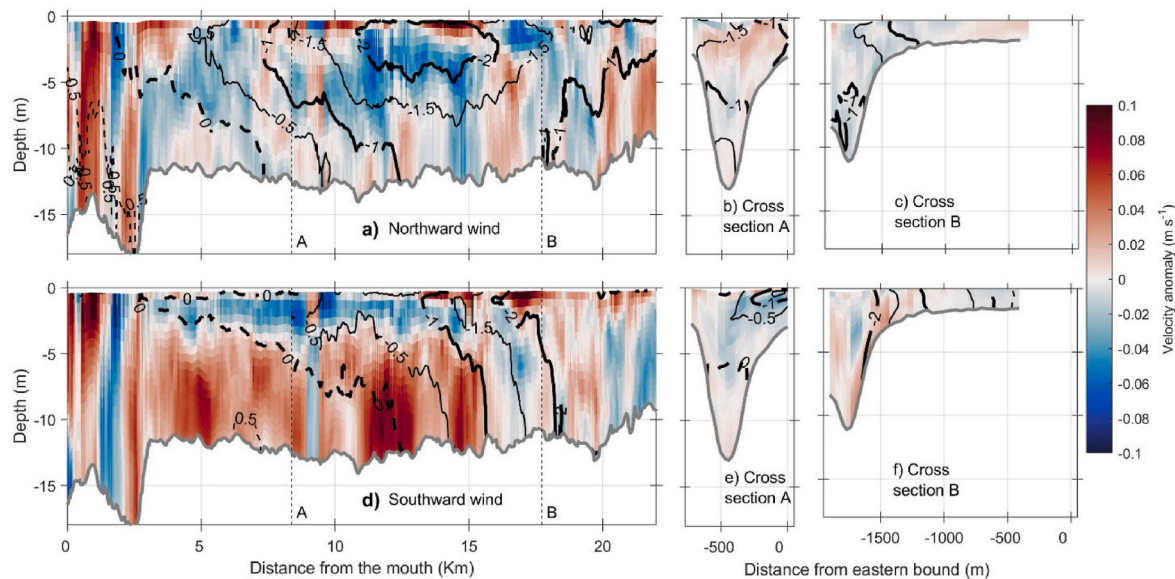


Fig. 9. Velocity (color) and salinity (lines) anomalies under moderate discharge, neap tides, and weak northward winds (top panels) and for weak southward winds (lower panels). (a, d) show velocity and salinity in the thalweg and locations of Cross sections, (b, e) show velocity and salinity anomalies at Cross section A, and (c, f) at Cross section B. Location of Cross sections are shown in Fig. 1b. (For interpretation of the references to color in this figure legend, the reader is referred to the Web version of this article.)

effects of southward winds on stratification and salinity gradient along the thalweg also changes spatially, especially due to the presence of North Bend (Fig. 8). When southward winds are applied, stratification near North Bend increases, similar to what is observed under northward winds (Fig. 8a, c, e). The change in stratification is tied to an increase in

salinity due to increased up-estuary flow at depth, which in turn also increases $\partial S/\partial x$ (Fig. 8b, d, f). Estuary-averaged salt shows that salinity initially decreases under high discharge, as winds are in the same direction as advection in Main Channel (Fig. 10a). After a day of wind influence, salinity begins to increase due to a strengthened exchange

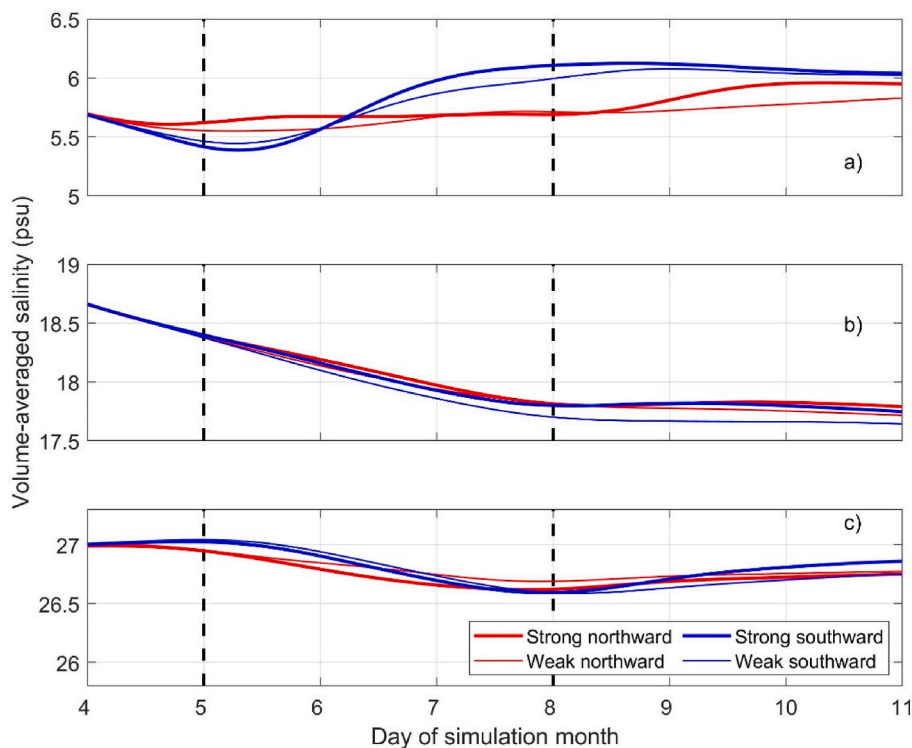


Fig. 10. (a) Temporal variability of volume-averaged salinity over the whole estuary for the high discharge case. Different colors represent the direction of the wind forcing, while the line width depends on strength of wind forcing. Broken vertical black lines show when the winds are turned on and off. (b) Same as in a, but for moderate discharge. (c) Same as in a, but for low discharge. (For interpretation of the references to color in this figure legend, the reader is referred to the Web version of this article.)

flow which brings saltier water at depth in most of the water column (not shown). Under moderate discharge, the accumulated fresher water in East Bay Channel (Fig. 9) is slowly exported from the estuary until salinity reaches a stable value of 17.7.

Interestingly, both wind directions increase the overall salinity of the estuary. However, the increase across the estuary is due to different processes: in the northward wind case, winds accumulate fresher waters in North Bend, due to reduced exchange flow in Main Channel and enhanced exchange flow in East Bay Channel, not allowing the fresher water out of the estuary. In the southward case, exchange flow is enhanced at the mouth due to wind straining at the surface and upwelling at depth, and secondary flow transports salt towards the shallow flats.

5. Discussion

Observations shown here indicate that despite the tidal dominance on setting the exchange flow magnitude in the Coos Estuary, strong winds can force reversals in surface velocities and influence the along-estuary salinity field (Figs. 2 and 4). Northward winds drive these reversal events in the Main Channel and occur more often under neap tide conditions (Fig. 2). The numerical simulations support the observations, showing that northward wind stress weakens the out-estuary flow at the surface along the thalweg in Main Channel, while on the shallower portions flow is reduced or even reversed (Fig. 9). Beyond the bend, the U-shaped geometry effectively reverses the direction of the wind's effect. That is, in East Bay Channel, northward winds act in the same direction as exchange flow at the surface, enhancing the exit of fresher water, leading to a pile-up of fresher water between 12 and 16 km. In contrast, southward winds shove surface waters towards the south, increasing the inflow of saltier waters along the northern boundaries of the estuary.

Our observations and modeling experiments show that despite the strong dependence of salinity gradient on river discharge and tidal forcing, winds can also affect the salinity gradient in the Coos Estuary (Fig. 8). When wind forcing is turned on, the overall salinity increases

under both northward and southward wind forcing, albeit with spatial and temporal variability (Fig. 10): northward winds increase the salinity gradient in Main Channel due to a piling of fresher waters in North Bend, while southward winds increase it in East Bay Channel due to a transport of fresher waters south and upwelling at the mouth. Although high discharge events occur only 25% of the time, the estuary response to winds is amplified during those conditions due to an increased stratification and salinity gradient (Fig. 8). Observations during northward winds (Fig. 4) show that these changes to salinity and velocity seem to be transient, due to the onset of increasing river discharge that coincides with the storm event. Longer-lasting winds occur as observed under upwelling-favorable southward winds.

In Main Channel at depth, the exchange flow resembles the dynamics of a relatively simpler estuarine geometry (Chen and Sanford, 2009; Li and Li, 2011; Monismith, 1986). However, due to both the presence of a complicated channel curvature and the abundant tidal flats, significant cross-estuary variability develops in East Bay. These results emphasize the spatial variability that wind induces on estuaries with complex geometries (e.g., Coogan et al., 2020; Guo and Valle-Levinson, 2008; Purkiani et al., 2016; Valle-Levinson et al., 2001), or ones with channel-flats geometries (Geyer et al., 2020; Ralston and Stacey, 2005), both of which are common in estuaries across the PNW and the globe.

5.1. Wind-induced temporal variability of salinity

Previously, the Coos Estuary was found to be unsteady due to both strong tidal forcing and short timescales of river discharge events (Conroy et al., 2020). By accounting for wind forcing, which was neglected previously but varies on even shorter time scales than the river discharge, the salinity and velocity that characterize the Coos Estuary are changed (Fig. 4). This combination of strong tides, episodic river forcing, and winds makes the Coos Estuary comparable to numerous other small, strongly forced systems (Banas et al., 2004; Lerczak et al., 2006; Ralston et al., 2010a; Simpson et al., 2001).

To explore the impacts of this unsteadiness, Chen and Sanford (2009) and Li and Li (2011) explored the impact of winds on the salt flux of an

idealized, partially-mixed estuary, and illustrated an important temporal variability attributed to the adjustment of sea level due to a barotropic seiche (advective flux). Our results also show a barotropic sea level adjustment due to water piled in North Bend under northward winds (Fig. 7b), and may explain the temporal variability of salinity in our observations (Fig. 4, Sup. Fig. 4). Additionally, Conroy et al. (2020) shows enhanced eulerian flux of salt in Main Channel due to higher levels of discharge, which affects the eulerian flux of salt. Our results show that under wind influence the exchange flow is affected due to winds being in opposite or the same direction at the surface. This additional eulerian flux would also increase the salinity gradient and shift salt flux towards the tidal and eulerian fluxes (Sup. Fig. 4).

5.2. Biological implications

Linkages between the physical and biological components of an estuary can be direct (e.g., currents advecting larvae through certain parts of a system), or indirect (e.g., changes to estuarine circulation lead to changes in temperature or salinity levels that affect organisms differently). Changes in the overall salt content of an estuary, whether due to river discharge, tides and/or winds, can thereby reduce or expand areas where larvae or other organisms can survive (Childers et al., 1990; Peterson, 2003; Teodósio et al., 2016). At the same time, changes in water level, including wind-driven changes, can decrease access of organisms to specific areas of an estuary where they can find shelter (Minello et al., 2012). Our study shows that wind forcing influences salinity in the Coos Estuary, with long-lasting changes (i.e., persistent days beyond the wind event, Fig. 4). Though in some cases the velocity returns to its original values after the winds have been turned off, the estuary-averaged salinity does not return to its pre-event values (Fig. 10). These significant changes occur especially when the river discharge falls within high (26% of the time) or moderate (45% of the time), accounting for >70% of each year. Additionally, there is enhanced salinity and velocity variability on tidal flats due to wind forcing, related to processes such as lateral trapping (Conroy et al., 2020; MacVean and Stacey, 2011; Okubo, 1973). Tidal flats in an estuary lead to ebb-tide dominance (Fortunato and Oliveira, 2005), and may be of much importance to the lateral salt flux in shallow, strongly stratified estuaries, such as the Coos or the San Francisco Bay (Ralston et al., 2010b; Ralston and Stacey, 2007), due to the abundant amount of shallow areas.

The transport of less-mobile organisms, such as larvae, can be enhanced by winds. For example, in Chesapeake Bay, Hare et al. (2005) showed that the up-estuary flux of young fish larvae was dominated by a combination of tidal, wind, and residual bottom inflow. Our results also show wind-enhanced transport when winds are blowing northwards (Fig. 10), with a stronger impact on the shallower parts of the estuary, e.g., stronger up-estuary flow on the eastern side of Main Channel (Fig. 7). In the southward wind cases, the exchange flow is strengthened at the surface in the out-estuary direction, enhancing up-estuary velocities at depth. This deep pathway may be a channel for larvae, phytoplankton, contaminants and other buoyant particles, to access the estuary. Recently, during 2014, an increased population of green crab larvae was found in areas up to North Bend (Yamada et al., 2020), and latitudinally as far north as Puget Sound (Grason et al., 2018). This anomalous transport of green crab populations has been related to changes in basin scale patterns, such as marine heatwaves (Peterson et al., 2017) and El Niños (Brasseale et al., 2019). Within an estuary, the effect of changes in climatological wind patterns could lead to up-estuary transport of organisms to outside their observed range. Indeed, many climate change scenarios predict intensified winds in the PNW (Bakun et al., 2015).

Roegner et al. (2007) also found a significant correlation between larval recruitment and tidal processes, showing that larvae entered South Slough during neap tides and not with spring tides, with slightly enhanced recruitment under upwelling (northward) winds. Our results show that during neap tides both stratification and salinity gradients

increase during the majority of forcing conditions allowing for larvae that are transported at depth to move further up-estuary (Fig. 5). This increase in stratification and salinity gradient, due to fortnightly variability, allows for a stronger susceptibility of the water column to winds (Wedderburn number, Chen and Sanford, 2009), in which the residence times of organisms may increase (Geyer, 1997).

6. Conclusions

Observations from a year-long velocity time-series in the Coos Estuary, OR, show that under northward wind stress, the normal out-estuary exchange-flow pattern is reversed at the surface, in part due to the inverted-U shape of the system. Salinity increases slightly in the estuary during the initial onset of these winds, before quickly freshening due to increased river discharge. Winds play two additional roles in the estuary, acting as an extra source of mixing that affect stratification and by piling up water that creates barotropic pressure gradients.

We conducted numerical experiments to investigate the spatial and temporal variability of wind effects on circulation and salinity of the Coos Estuary, by looking at specific combinations of tides, river discharge and winds. Despite the idealized forcing, salinity gradients and stratification show good agreement with observations. When winds blow northward, fresher water piles up on the north side of the estuary, while there is an asymmetric response in velocity: a reduction in Main Channel, due to winds opposing the exchange flow, while beyond North Bend, winds enhance the out-estuary circulation at the surface. In the case of southward winds, we find an asymmetric response in salinity, as salt is pushed out-estuary at the surface in Main Channel, increasing stratification, while beyond North Bend, the same winds keep fresher waters accumulated up-estuary.

The wind impact on stratification and salinity gradient alter salt fluxes in a non-transient way that has a strong dependence on the river discharge. Under high discharge, most of the impact of winds occurs in Main Channel, where winds exert opposite effects on the surface velocity: northward winds are in the opposite direction as exchange flow and the barotropic pressure gradient, while southward winds are in the same direction as both. After the winds relax, the accumulated fresh water exits the estuary at the surface while strengthened exchange flow at depth increases salinity slightly. Southward winds result in a saltier lower layer due to upwelling at the mouth. During moderate and low discharge conditions, we find a similar response to wind. However, due to reduced stratification and along-estuary salinity gradient, the effect on the salinity field is smaller, resulting in a smaller anomalous salt loss out-estuary and reaching a stable salinity after the winds stop.

CRedit authorship contribution statement

Maria Jose Marin Jarrin: Writing – original draft, Visualization, Methodology, Formal analysis, Conceptualization. **David A. Sutherland:** Writing – review & editing, Supervision, Resources, Funding acquisition, Conceptualization.

Declaration of competing interest

The authors declare that they have no known competing financial interests or personal relationships that could have appeared to influence the work reported in this paper.

Data availability

Data will be made available on request.

Acknowledgments

This work was sponsored by the National Estuarine Research Reserve System Science Collaborative, which supports collaborative research

that addresses coastal management problems important to the reserves. The Science Collaborative is funded by the National Oceanic and Atmospheric Administration and managed by the University of Michigan Water Center (NAI4NOS4190145). This work benefited from access to the University of Oregon high performance computer, Talapas. We would like to thank Dave Ralston and Emily Eidam for comments on an earlier draft, as well as 3 anonymous reviewers and the journal editor.

Appendix A. Supplementary data

Supplementary data to this article can be found online at <https://doi.org/10.1016/j.ecss.2022.108092>.

References

- Bakun, A., Black, B., Bograd, S.J., García-Reyes, M., Miller, a.J., Rykaczewski, R.R., Sydeman, W.J., 2015. Anticipated effects of climate change on coastal upwelling ecosystems. *Curr. Clim. Change Rep.* 85–93. <https://doi.org/10.1007/s40641-015-0008-4>.
- Banas, N.S., Hickey, B.M., MacCready, P., Newton, J.A., 2004. Dynamics of Willapa Bay, Washington: a highly unsteady, partially mixed estuary. *J. Phys. Oceanogr.* 34, 2413–2427. <https://doi.org/10.1175/JPO2637.1>.
- Banas, N.S., McDonald, P.S., Armstrong, D.A., 2009. Green crab larval retention in Willapa Bay, Washington: an intensive Lagrangian modeling approach. *Estuar. Coast* 32, 893–905. <https://doi.org/10.1007/s12237-009-9175-7>.
- Baptista, A.M., 1989. Salinity in Coos Bay, Oregon. OR, Portland.
- Blumberg, A.F., Goodrich, D.M., 1990. Modeling of wind-induced destratification in Chesapeake Bay. *Estuaries* 13, 236. <https://doi.org/10.2307/1351914>.
- Bolaños, R., Brown, J.M., Amoudry, L.O., Souza, A.J., 2013. Tidal, riverine, and wind influences on the circulation of a macrotidal estuary. *J. Phys. Oceanogr.* 43, 29–50. <https://doi.org/10.1175/JPO-D-11-0156.1>.
- Brasseale, E., Grason, E.W., McDonald, P.S., Adams, J., MacCready, P., 2019. Larval transport modeling support for identifying population sources of European green crab in the salish sea. *Estuar. Coast* 42, 1586–1599. <https://doi.org/10.1007/s12237-019-00586-2>.
- Chant, R.J., 2002. Secondary circulation in a region of flow curvature: relationship with tidal forcing and river discharge. *J. Geophys. Res.* 107, 3131. <https://doi.org/10.1029/2001JC001082>.
- Chen, C., Liu, H., Beardsley, R.C., 2003. An unstructured grid, finite-volume, three-dimensional, primitive equations ocean model: application to coastal ocean and estuaries. *J. Atmos. Ocean. Technol.* 20, 159–186. [https://doi.org/10.1175/1520-0426\(2003\)020<0159:AUGVT>2.0.CO;2](https://doi.org/10.1175/1520-0426(2003)020<0159:AUGVT>2.0.CO;2).
- Chen, S.-N., Sanford, L.P., 2009. Axial wind effects on stratification and longitudinal salt transport in an idealized, partially mixed estuary. *J. Phys. Oceanogr.* 39, 1905–1920. <https://doi.org/10.1175/2009jpo4016.1>.
- Chen, T., Zhang, Q., Wu, Y., Ji, C., Yang, J., Liu, G., 2018. Development of a wave-current model through coupling of FVCOM and SWAN. *Ocean Eng.* 164, 443–454. <https://doi.org/10.1016/j.oceaneng.2018.06.062>.
- Childers, D.L., Day, J.W., Muller, R.A., 1990. Relating climatological forcing to coastal water levels in Louisiana estuaries and the potential importance of El Niño-Southern Oscillation events. *Clim. Res.* 1, 31–42. <https://doi.org/10.3354/cr001031>.
- Cloern, J.E., Jassby, A.D., Schraga, T.S., Nejad, E., Martin, C., 2017. Ecosystem variability along the estuarine salinity gradient: examples from long-term study of San Francisco Bay. *Limnol. Oceanogr.* 62, 1053–1057. <https://doi.org/10.1002/lno.10537>.
- Conroy, T., Sutherland, D.A., Ralston, D.K., 2020. Estuarine exchange flow variability in a seasonal, segmented estuary. *J. Phys. Oceanogr.* 50, 595–613. <https://doi.org/10.1175/JPO-D-19-0108.1>.
- Coogan, J., Dzwonkowski, B., 2018. Observations of wind forcing effects on estuary length and salinity flux in a river-dominated, microtidal Estuary, Mobile Bay, Alabama. *J. Phys. Oceanogr.* 48, 1787–1802. <https://doi.org/10.1175/JPO-D-17-0249.1>.
- Coogan, J., Dzwonkowski, B., Park, K., Webb, B., 2020. Observations of restratification after a wind mixing event in a shallow highly stratified estuary. *Estuar. Coast* 43, 272–285. <https://doi.org/10.1007/s12237-019-00689-w>.
- Csanady, G.T., 1973. Wind-induced barotropic motions in long lakes. *J. Phys. Oceanogr.* 3, 429–438. [https://doi.org/10.1175/1520-0485\(1973\)003<0429:WIBMIL>2.0.CO;2](https://doi.org/10.1175/1520-0485(1973)003<0429:WIBMIL>2.0.CO;2).
- Eidam, E.F., Sutherland, D.A.A., Ralston, D.K.K., Dye, B., Conroy, T., Schmitt, J., Ruggiero, P., Wood, J., 2020. Impacts of 150 Years of Shoreline and Bathymetric Change in the Coos Estuary, Oregon, USA. *Estuaries and Coasts*. <https://doi.org/10.1007/s12237-020-00732-1>.
- Emmett, R., Llansó, R., Newton, J., Thom, R.M., Hornberger, M., Morgan, C., Levings, C., Copping, A., Fishman, P., Llansó, R., 2000. Geographic signatures of North American West Coast estuaries. *Estuaries* 23, 765. <https://doi.org/10.2307/1352998>.
- Epifanio, C.E., Garvine, R.W., 2001. Larval transport on the atlantic continental shelf of North America: a review. *Estuar. Coast Shelf Sci.* 52, 51–77. <https://doi.org/10.1006/ecss.2000.0727>.
- Fortunato, A.B., Oliveira, A., 2005. Influence of intertidal flats on tidal asymmetry. *J. Coast Res.* 215, 1062–1067. <https://doi.org/10.2112/03-0089.1>.
- Garvine, R.W., 1991. Subtidal frequency estuary-shelf interaction: observations near Delaware bay. *J. Geophys. Res.* 96, 7049–7064. <https://doi.org/10.1029/91jc00079>.
- Geyer, 1997. Influence of wind on dynamics and flushing of shallow estuaries. *Estuar. Coast Shelf Sci.* 44, 713–722. <https://doi.org/10.1006/ecss.1996.0140>.
- Geyer, W.R., 1997. Influence of wind on dynamics and flushing of shallow estuaries. *Estuar. Coast Shelf Sci.* 44, 713–722. <https://doi.org/10.1006/ecss.1996.0140>.
- Geyer, W.R., 1993. Three-dimensional tidal flow around headlands. *J. Geophys. Res. Ocean.* 98, 955–966. <https://doi.org/10.1029/92JC02270>.
- Geyer, W.R., Ralston, D.K., Chen, J., 2020. Mechanisms of exchange flow in an estuary with a narrow, deep channel and wide, shallow shoals. *J. Geophys. Res. Ocean.* 1–25. <https://doi.org/10.1029/2020jc016092>.
- Giddings, S.N., MacCready, P., 2017. Reverse estuarine circulation due to local and remote wind forcing, enhanced by the presence of along-coast estuaries. *J. Geophys. Res. Ocean.* 122, 10184–10205. <https://doi.org/10.1002/2016JC012479>.
- Grason, E., McDonald, S., Adams, J., Little, K., Apple, J., Pleus, A., 2018. Citizen science program detects range expansion of the globally invasive European green crab in Washington State (USA). *Manag. Biol. Invasions* 9, 39–47. <https://doi.org/10.3391/mbi.2018.9.1.04>.
- Groth, S., Rumrill, S., 2009. History of Olympia oysters (*Ostrea lurida* Carpenter 1864) in Oregon estuaries, and a description of recovering populations in Coos bay. *J. Shellfish Res.* 28, 51–58. <https://doi.org/10.2983/035.028.0111>.
- Guo, X., Valle-Levinson, A., 2008. Wind effects on the lateral structure of density-driven circulation in Chesapeake Bay. *Contin. Shelf Res.* 28, 2450–2471. <https://doi.org/10.1016/j.csr.2008.06.008>.
- Hansen, D.V., Rattray, M., 1965. Gravitational circulation in straits and estuaries. *J. Mar. Res.* 23, 104–122. <https://doi.org/10.1098/rspb.2009.2214>.
- Hare, J.A., Thorrold, S., Walsh, H., Reiss, C., Valle-Levinson, A., Jones, C., 2005. Biophysical mechanisms of larval fish ingress into Chesapeake Bay. *Mar. Ecol. Prog. Ser.* 303, 295–310. <https://doi.org/10.3354/meps303295>.
- Hickey, B., Geier, S., Kachel, N., Ramp, S., Kosro, P.M., Connolly, T., 2016. Alongcoast structure and interannual variability of seasonal midshelf water properties and velocity in the Northern California Current System. *J. Geophys. Res. Ocean.* 121, 7408–7430. <https://doi.org/10.1002/2015JC011424>.
- Hickey, B.M., Banas, N.S., 2003. Oceanography of the U. S. Pacific northwest coastal ocean and estuaries with application to coastal ecology. *Estuaries* 26, 1010–1031.
- Huang, H., Chen, C., Cowles, G.W., Winant, C.D., Beardsley, R.C., Hedstrom, K.S., Haidvogel, D.B., 2008. FVCOM validation experiments: comparisons with ROMS for three idealized barotropic test problems. *J. Geophys. Res. Ocean.* 113, 1–14. <https://doi.org/10.1029/2007JC004557>.
- Janzen, C.D., Wong, K.-C., 2002. Wind-forced dynamics at the estuary-shelf interface of a large coastal plain estuary. *J. Geophys. Res. Ocean.* 107, 3138. <https://doi.org/10.1029/2001JC000959>.
- Kranenburg, W.M., Geyer, W.R., Garcia, A.M.P., Ralston, D.K., 2019. Reversed lateral circulation in a sharp estuarine bend with weak stratification. *J. Phys. Oceanogr.* 49, 1619–1637. <https://doi.org/10.1175/JPO-D-18-0175.1>.
- Lacy, J.R., Monismith, S.G., 2001. Secondary currents in a curved, stratified, estuarine channel. *J. Geophys. Res. Ocean.* 106, 31283–31302. <https://doi.org/10.1029/2000JC000606>.
- Lee, H., Brown, C.A., 2009. Classification of Regional Patterns of Environmental Drivers and Benthic Habitats in Pacific Northwest Estuaries.
- Lerczak, J.A., Geyer, W.R., 2004. Modeling the lateral circulation in straight, stratified estuaries. *J. Phys. Oceanogr.* 34, 1410–1428. [https://doi.org/10.1175/1520-0485\(2004\)034<1410:MTLCLIS>2.0.CO;2](https://doi.org/10.1175/1520-0485(2004)034<1410:MTLCLIS>2.0.CO;2).
- Lerczak, J.A., Geyer, W.R., Chant, R.J., 2006. Mechanisms driving the time-dependent salt flux in a partially stratified estuary. *J. Phys. Oceanogr.* 36, 2296–2311. <https://doi.org/10.1175/JPO2959.1>.
- Li, Y., Li, M., 2011. Effects of winds on stratification and circulation in a partially mixed estuary. *J. Geophys. Res. Ocean.* 116. <https://doi.org/10.1029/2010JC006893>.
- MacCready, P., Geyer, W.R., 2010. Advances in estuarine physics. *Ann. Rev. Mar. Sci.* 2, 35–58. <https://doi.org/10.1146/annurev-marine-120308-081015>.
- MacVean, L.J., Stacey, M.T., 2011. Estuarine dispersion from tidal trapping: a new analytical framework. *Estuar. Coast* 34, 45–59. <https://doi.org/10.1007/s12237-010-9298-x>.
- Minello, T.J., Rozas, L.P., Baker, R., 2012. Geographic variability in salt marsh flooding patterns may affect nursery value for fishery species. *Estuar. Coast* 35, 501–514. <https://doi.org/10.1007/s12237-011-9463-x>.
- Monismith, S., 1986. An experimental study of the upwelling response of stratified reservoirs to surface shear stress. *J. Fluid Mech.* 171, 407. <https://doi.org/10.1017/S0022112086001507>.
- Nidzieko, N.J., Monismith, S.G., 2013. Contrasting seasonal and fortnightly variations in the circulation of a seasonally inverse estuary, Elkhorn slough, California. *Estuar. Coast* 36, 1–17. <https://doi.org/10.1007/s12237-012-9548-1>.
- O'Higgins, T., Rumrill, S.S., 2007. Tidal and watershed forcing of nutrients and dissolved oxygen stress within four Pacific coast estuaries: analysis of time-series data collected by the national estuarine research Reserve system-wide monitoring program (2000–2006) within Padilla bay (WA). NOAA/UNH Coop. Inst. Coast. Estuar. Environ. Technol. 1689–1699. <https://doi.org/10.1017/CBO9781107415324.004>.
- Officer, C.B., 1976. *Physical Oceanography of Estuaries (And Associated Coastal Waters)*. John Wiley, New York, US.
- Okubo, A., 1973. Effect of shoreline irregularities on streamwise dispersion in estuaries and other embayments. *NJSR (Neth. J. Sea Res.)* 6, 213–224. [https://doi.org/10.1016/0077-7579\(73\)90014-8](https://doi.org/10.1016/0077-7579(73)90014-8).
- Pawlowicz, R., Beardsley, R.C., Lentz, S.J., 2002. *Classical Tidal Harmonic Analysis Including Error Estimates in MATLAB Using T TIDE* 5, 28, pp. 929–937.
- Peterson, M.S., 2003. A conceptual view of environment-habitat-production linkages in tidal river estuaries. *Rev. Fish. Sci.* 11, 291–313. <https://doi.org/10.1080/10641260390255844>.

- Peterson, W.T., Fisher, J.L., Strub, P.T., Du, X., Risien, C., Peterson, J., Shaw, C.T., 2017. The pelagic ecosystem in the Northern California Current off Oregon during the 2014–2016 warm anomalies within the context of the past 20 years. *J. Geophys. Res. Ocean.* 122, 7267–7290. <https://doi.org/10.1002/2017JC012952>.
- Pfeiffer-Herbert, A.S., Kincaid, C.R., Bergondo, D.L., Pockalny, R.A., 2015. Dynamics of wind-driven estuarine-shelf exchange in the Narragansett Bay estuary. *Continent. Shelf Res.* 105, 42–59. <https://doi.org/10.1016/j.csr.2015.06.003>.
- Purkiani, K., Becherer, J., Klingbeil, K., Burchard, H., 2016. Wind-induced variability of estuarine circulation in a tidally energetic inlet with curvature. *J. Geophys. Res. Ocean.* 121, 3261–3277. <https://doi.org/10.1002/2015JC010945>.
- Qi, J., Chen, C., Beardsley, R.C., Perrie, W., Cowles, G.W., Lai, Z., 2009. An unstructured-grid finite-volume surface wave model (FVCOM-SWAVE): implementation, validations and applications. *Ocean Model.* 28, 153–166. <https://doi.org/10.1016/j.ocemod.2009.01.007>.
- Ralston, D.K., Geyer, W.R., Lerczak, J.A., 2010a. Structure, variability, and salt flux in a strongly forced salt wedge estuary. *J. Geophys. Res.* 115, C06005 <https://doi.org/10.1029/2009JC005806>.
- Ralston, D.K., Geyer, W.R., Lerczak, J.A., Scully, M., 2010b. Turbulent mixing in a strongly forced salt wedge estuary. *J. Geophys. Res. Ocean.* 115, 1–19. <https://doi.org/10.1029/2009JC006061>.
- Ralston, D.K., Stacey, M.T., 2007. Tidal and meteorological forcing of sediment transport in tributary mudflat channels. *Continent. Shelf Res.* 27, 1510–1527. <https://doi.org/10.1016/j.csr.2007.01.010>.
- Ralston, D.K., Stacey, M.T., 2005. Longitudinal dispersion and lateral circulation in the intertidal zone. *J. Geophys. Res. C Oceans* 110, 1–17. <https://doi.org/10.1029/2005JC002888>.
- Roegner, G.C., Armstrong, D.A., Shanks, A.L., 2007. Wind and tidal influences on larval crab recruitment to an Oregon estuary. *Mar. Ecol. Prog. Ser.* 351, 177–188. <https://doi.org/10.3354/meps07130>.
- Sanay, R., Valle-Levinson, A., 2005. Wind-induced circulation in semienclosed homogeneous, rotating basins. *J. Phys. Oceanogr.* 35, 2520–2531. <https://doi.org/10.1175/JPO2831.1>.
- Scully, M.E., Friedrichs, C., Brubaker, J., 2005. Control of estuarine stratification and mixing by wind-induced straining of the estuarine density field. *Estuaries* 28, 321–326. <https://doi.org/10.1007/BF02693915>.
- Sharples, J., Middelburg, J.J., Fennel, K., Jickells, T.D., 2017. What proportion of riverine nutrients reaches the open ocean? *Global Biogeochem. Cycles* 31, 39–58. <https://doi.org/10.1002/2016GB005483>.
- Simpson, J.H., Vennell, R., Souza, A.J., 2001. The salt fluxes in a tidally-energetic estuary. *Estuar. Coast Shelf Sci.* 52, 131–142. <https://doi.org/10.1006/ecss.2000.0733>.
- Sutherland, D.A., O'Neill, M.A., 2016. Hydrographic and dissolved oxygen variability in a seasonal Pacific Northwest estuary. *Estuar. Coast Shelf Sci.* 172, 47–59. <https://doi.org/10.1016/j.ecss.2016.01.042>.
- Teodósio, M.A., Paris, C.B., Wolanski, E., Morais, P., 2016. Biophysical processes leading to the ingress of temperate fish larvae into estuarine nursery areas: a review. *Estuar. Coast Shelf Sci.* 183, 187–202. <https://doi.org/10.1016/j.ecss.2016.10.022>.
- U.S. Army Corps of Engineers, 2015. COOS BAY FEDERAL NAVIGATION CHANNEL and CHARLESTON SIDE CHANNEL Dredging Project. OR, Portland.
- Uncles, R.J., Stephens, J.A., 2011. The effects of wind, runoff and tides on salinity in a strongly tidal Sub-estuary. *Estuar. Coast* 34, 758–774. <https://doi.org/10.1007/s12237-010-9365-3>.
- Valle-Levinson, A., Schettini, C.A.F., Truccolo, E.C., 2019. Subtidal variability of exchange flows produced by river pulses, wind stress and fortnightly tides in a subtropical stratified estuary. *Estuar. Coast Shelf Sci.* 221, 72–82. <https://doi.org/10.1016/j.ecss.2019.03.022>.
- Valle-Levinson, A., Wong, K.-C., Bosley, K.T., 2001. Observations of the wind-induced exchange at the entrance to Chesapeake Bay. *J. Mar. Res.* 59, 391–416. <https://doi.org/10.1357/002224001762842253>.
- Xia, M., Xie, L., Pietrafesa, L.J., Whitney, M.M., 2011. The ideal response of a Gulf of Mexico estuary plume to wind forcing: its connection with salt flux and a Lagrangian view. *J. Geophys. Res.* 116, C08035 <https://doi.org/10.1029/2010JC006689>.
- Xie, L., Eggleston, D.B., 1999. Computer simulations of wind-induced estuarine circulation patterns and estuary-shelf exchange processes: the potential role of wind forcing on larval transport. *Estuar. Coast Shelf Sci.* 49, 221–234. <https://doi.org/10.1006/ecss.1999.0498>.
- Yamada, S.B., Dumbauld, B.R., Kalin, A., Hunt, C.E., Figlar-Barnes, R., Randall, A., 2005. Growth and persistence of a recent invader *Carcinus maenas* in estuaries of the northeastern Pacific. *Biol. Invasions* 7, 309–321. <https://doi.org/10.1007/s10530-004-0877-2>.
- Yamada, S.B., Randall, A., Schooler, S., Heller, R., Donaldson, L., Takacs, G., Buffington, C., Akmajian, A., 2020. Status of the European Green Crab, *Carcinus maenas*, in Oregon and Washington Coastal Estuaries in 2019, Report Prepared for the Aquatic Nuisance Species Project. Portland, OR.